X. PLASMA PHYSICS*

Prof. S. C. Brown
Prof. W. P. Allis
Prof. G. Bekefi
Prof. D. R. Whitehouse
Prof. S. Gruber
V. Arunasalam
C. D. Buntschuh
J. F. Clarke
J. D. Coccoli
F. X. Crist
H. Fields
E. W. Fitzgerald, Jr.
P. J. Freyheit
W. H. Glenn, Jr.
E. B. Hooper, Jr.
J. C. Ingraham
J. J. McCarthy
S. J. Majumdar
W. J. Mulligan
J. J. Nolan, Jr.
H. R. Radoski
G. L. Rogoff
R. E. Whitney

A. NEGATIVE CONDUCTIVITY

Investigation of the conditions for a plasma to exhibit negative conductivity[1] in the presence of a magnetic field has been continued. Previously the conductivity of a weak plasma, solved from the Boltzmann equation by the standard perturbation method,[2] led to the absorption coefficient in the presence of a magnetic field

$$\alpha = -\frac{16\pi^4 c^2}{\omega^2 m}\int_0^\infty v_\perp\, dv_\perp \int_{-\infty}^{\infty} dv_\parallel\, \eta(\omega, \omega_b, \bar{v})\left[\frac{\partial f}{\partial v_\perp} - \frac{\cos\theta}{c}\left(\frac{v_\parallel \partial f}{\partial v_\perp} - \frac{\partial f}{v_\perp \partial v_\parallel}\right)\right] \tag{1}$$

where

$\eta(\omega, \omega_b, \bar{v})$ is the emission of a single particle in the plasma.
f is the unperturbed distribution function.
c is the velocity of light.
θ is the angle of propagation with respect to the magnetic field.
$v_\parallel$ is the particle velocity component along the magnetic field
$v_\perp$ is the particle velocity component perpendicular to the magnetic field.

The term $\left(\frac{v_\parallel \partial f}{\partial v_\perp} - \frac{v_\perp \partial f}{\partial v_\parallel}\right)\frac{\cos\theta}{c}$ arises from the interaction of the zeroth-order particle velocity with the magnetic field of the propagating plane wave whose angular frequency is ω. Previously the consideration of negative conductivity was limited to a discussion of the absorption coefficient for an isotropic but non-Maxwellian velocity distribution. Under these circumstances, this term is zero. We now examine the effect of the inclusion of this term in detail when the particles are considered to be nonrelativistic, and we also infer the effect on its inclusion when the effect of relativistic mass change is included in the search for negative conductivity.

*This work was supported in part by the Atomic Energy Commission under Contract AT(30-1)1842; in part by the Air Force Cambridge Research Center under Contract AF-19(604)-5992; and in part by the National Science Foundation (Grant G-9330).

A further word about the motivation of this calculation which was considered by Sagdeev and Shafranov[3] but in a different light than we do now. Recently, Chow and Pantell[4] have reported both amplification and oscillation at the cyclotron frequency in a configuration in which they employed a high-energy electron beam drifting in a waveguide. The beam energy was approximately 3000 volts and most of its energy was in the direction transverse to the magnetic field. The gain mechanism was explained by the consideration of the interaction of the ac magnetic field of a uniform plane wave upon the motion of the beam electrons. In this report we investigate the Chow-Pantell "fast-wave" amplification mechanism, using the equation for the absorption coefficient.

To simulate the distribution function of electron beam, we use

$$f = f_\perp f_\parallel = \frac{n}{\overline{v_\perp^2}} \exp\left(-\frac{(v_\perp - \overline{v}_\perp)^2}{2\overline{v_\perp^2}}\right) \frac{1}{\sqrt{2\pi\overline{v_\parallel^2}}} \exp\left(-\frac{(v_\parallel - \overline{v}_\parallel)^2}{2\overline{v_\parallel^2}}\right)$$

where $\overline{v_\perp^2}$, $\overline{v_\parallel^2}$ are the mean-square thermal velocities in the transverse and longitudinal directions, respectively, and $\overline{v}_\perp$, $\overline{v}_\parallel$ are the mean or drift velocities of the beam or plasma electrons in the transverse and longitudinal directions. An electron beam will be described as

$$\overline{v}_\perp \gg \sqrt{\overline{v_\perp^2}} \quad \text{and} \quad \overline{v}_\parallel \gg \sqrt{\overline{v_\parallel^2}} \ .$$

The emission of a collisionless plasma is given by

$$\eta = \frac{Kev_\perp^2}{\epsilon_o} (1+\cos^2\theta)\ \delta\left(\frac{\omega - kv_\parallel \cos\theta}{\omega_b} - 1\right) ,$$

where K is a constant, and $k = \omega/c$. Using these quantities in Eq. 1, we obtain

$$\alpha = \frac{16\pi^4 c^2 (1+\cos^2\theta)}{\omega^2 m\epsilon_o} Ke \int_0^\infty f_\perp v_\perp^3\, dv_\perp$$

$$\int_{-\infty}^{\infty} dv_\parallel \left[\frac{v_\perp - \overline{v}_\perp}{\overline{v_\perp^2}} + \frac{v_\perp |\cos\theta|}{c} \frac{v_\parallel - \overline{v}_\parallel}{\overline{v_\parallel^2}}\right] f_\parallel\, \delta\left(\frac{\omega - kv_\parallel \cos\theta}{\omega_b} - 1\right) . \qquad (2)$$

The term $\frac{v_\parallel \cos\theta}{c}$ is always negligible as compared with unity, and so we have dropped it from the integral in this context.

The integral over $v_\parallel$ may be performed for propagation angles less than 90° to obtain

$$\alpha = + A \int_0^\infty v_\perp^3 f_\perp \left[\frac{v_\perp (1+B) - \bar{v}_\perp}{\overline{v_\perp^2}} \right] dv_\perp . \tag{3}$$

Here, for compactness, we have defined

$$A = n \frac{16 \pi^4 c^2 (1+\cos^2 \theta)}{\omega^2 m \epsilon_o \sqrt{2\pi \overline{v_\parallel^2}}} eK \frac{\omega_b}{k|\cos \theta|} \exp - \left[\left(\frac{\omega - \omega_b}{k \cos \theta} - \bar{v}_\parallel \right)^2 / 2\overline{v_\parallel^2} \right]$$

and

$$B = \left[\frac{\left(\frac{\omega - \omega_b}{k \cos \theta} \right) - \bar{v}_\parallel}{c} \right] \frac{\overline{v_\perp^2}}{\overline{v_\parallel^2}} |\cos \theta| .$$

We now perform the integration on $v_\perp$ to find in two limiting, but not too restrictive, cases.

Case I: $\bar{v}_\perp = 0$

In this case, in order to conserve particles, we must multiply the distribution function by 2, and integrate to find

$$\alpha = A(1+B) \left(\overline{v_\perp^2} \right)^{3/2} \Gamma (5/2) \frac{2\sqrt{2}}{\overline{v_\perp^2}} .$$

Since A is always positive, gain can only be obtained if $B < -1$. This can occur if

$$\frac{\omega_b - \omega}{k \cos \theta} + \bar{v}_\parallel > \frac{\overline{v_\parallel^2}}{\overline{v_\perp^2}} \times c ,$$

a condition that can only occur when the thermal spread along the magnetic field is very small compared with that transverse to it, for the quantity on the left of the inequality may be several times the longitudinal thermal velocity (otherwise A becomes negligibly small). If we set the left-hand side of this inequality equal to $\sqrt{\overline{v_\parallel^2}}$, then we have the condition for gain (negative α):

$$\overline{v_\perp^2} > c \sqrt{\overline{v_\parallel^2}} . \tag{4}$$

As an example, let the temperature in the longitudinal direction be 0.01 ev; then the transverse temperature should be approximately 100 ev. A longitudinal energy of 1 ev requires a transverse temperature of approximately 1000 ev. We expect that under

these conditions relativistic effects should have been included.

Case II: $\bar{v}_\perp \gg \sqrt{\overline{v_\perp^2}}$

The integration yields, to a very good approximation,

$$a \approx n \frac{16\pi^4 (1+\cos^2\theta)\, Ke\, (\omega_b/k)c}{\omega^2 m\epsilon_o \sqrt{2\pi \overline{v_\parallel^2}}} \left(\frac{\omega-\omega_b}{k\cos\theta} - \bar{v}_\parallel \right)$$

$$\times \frac{\overline{v_\perp^2}}{\overline{v_\parallel^2}} \sqrt{2\pi \overline{v_\perp^2}}\, \exp - \left[\left(\frac{\omega-\omega_b}{k\cos\theta} - \bar{v}_\parallel \right)^2 / 2\overline{v_\parallel^2} \right]. \tag{5}$$

This yields gain if

$$\frac{\omega_b - \omega}{\omega} > \frac{\bar{v}_\parallel \cos\theta}{c}, \tag{6}$$

which might be called a "slippage" condition.

Recall that in the derivation of Eq. 5 we considered that the propagation direction did not include $\theta = \pi/2$. In fact, when $\theta \approx \frac{\pi}{2} - \frac{1}{2}\frac{\overline{v}_\parallel^2}{c^2}$ we must take into account relativistic effects in the delta function. That is, we must replace ω_b with $\omega_{b_o}\sqrt{1-\frac{v_\perp^2+v_\parallel^2}{c^2}}$, and complications result. In the first place, if we assume that $\frac{v_\parallel^2}{2c^2} \ll \frac{v_\parallel}{c}\cos\theta$ and retain the relativistic effect in the transverse energy, we find that over a wide range of thermal energy in the longitudinal direction the dominant effect is not the relativistic term but the interaction with the ac magnetic field. An estimate of this range may be obtained from the width in $v_\perp$ of the result of integrating Eq. 2 on $v_\parallel$. That is, the factor

$$\exp - \left[\left(\frac{\omega-\omega_b\left(1-\frac{v_\perp^2}{2c^2}\right)}{k\cos\theta} \right) - \bar{v}_\parallel^2 / 2\overline{v_\parallel^2} \right]$$

should have a smaller width than that of $f_\perp$ for the variation of the former with $v_\perp$ to be important during the secnod integration. This yields the condition

$$\left(\overline{v_\perp^2}\right)^2 > 8\overline{v_\parallel^2} c^2 \cos^2\theta \tag{7}$$

which if it is satisfied means that relativistic effects must be included. We see that

condition (4) implies that we must include relativistic effects when considering gain in Case I.

Calculation of the gain in Case II as given by Eq. 7 is under way and will be compared with the data of Chow and Pantell.

S. Gruber

References

1. G. Bekefi, J. L. Hirshfield, and S. C. Brown, Kirchhoff Radiation Law for plasmas with non-Maxwellian distributions, Phys. Fluids 4, 173-176 (1961).

2. S. Gruber, Negative conductivity in a plasma, Quarterly Progress Report No. 61, Research Laboratory of Electronics, M. I. T., April 15, 1961, pp. 5-10.

3. R. Z. Sagdeev and V. D. Shafranov, Soviet Phys.—JETP 12, 130 (1961).

4. K. K. Chow and R. H. Pantell, Report 800, Microwave Laboratory, Stanford University, Stanford, California, 1961.

B. ELECTRON TEMPERATURE DECAY IN HELIUM PLASMA AFTERGLOW

The transient microwave radiation pyrometer[1] with the modifications described below has been used to study the build-up and decay of the electron radiation temperature[2] in a pulsed gas discharge in helium gas.

The modifications are: a lower pulse frequency (200 sec^{-1} instead of 1000 sec^{-1}) and a provision to alter this rate with a minimum of difficulty; discharge current pulses variable from 5 μsec to 1250 μsec in duration instead of only 200-300 μsec; discharge current amplitude variable from 5 ma to 1200 ma instead of a maximum of 300 ma; and provision for measuring the radiation temperature throughout the whole of the build-up and decay of the plasma, instead of only the period beginning 2 μsec after the termination of the discharge current. These modifications were intended to eliminate transients in the discharge caused by breakdown, to investigate these transients, and to better determine the initial conditions of the afterglow period.

The first observations were of the temperature of the developing discharge as a function of time. The general features for 2.45 mm pressure and a 1.3-cm diameter discharge tube are:

(a) A very high temperature (~50,000°) is initially observed which drops to a minimum (~15,000°) at 200-300 μsec, and then increases sometimes oscillating before settling down at approximately 500 μsec (~26,000°).

(b) When temperature decay was observed with a pulse length between 200-300 μsec the temperature actually increased before decaying; this indicates that the temperature oscillations are probably caused by moving temperature gradients.

(c) The actual leveling-off of the temperature at 500 μsec refers to a point at which

the discharge characteristics are no longer repeatable from pulse to pulse so that fluctuating phenomena will average to zero. Observations of the density fluctuations indicate that the amplitude of the fluctuations is just as large in the nonrepeatable region.

These density gradients were observed visually, and by detecting the power reflected from the discharge from a 7500-mc source incident normal to the discharge tube. For short duration discharge pulses, the areas of brightness appeared to be at fixed positions in the tube, probably near the point where they were at the instant of termination of the discharge. These positions moved toward the cathode as the pulse was lengthened. We take this as an indication that these temperature and density gradients are moving from anode to cathode.

Other temperature-decay measurements were made to supplement earlier measurements.[1] Investigation of these curves (old and new data) showed that for low electron densities the temperature in the late afterglow decayed exponentially with time with a time constant that agreed fairly well with the diffusion time for helium metastables over the pressure range 0.2-1 mm.[3]

These equations govern the helium afterglow (we assume only ambipolar diffusion loss for electrons):

$$\frac{dn_e}{dt} = \frac{n_e}{\tau_e}, \tag{1}$$

$$\frac{dn_m}{dt} = -\frac{n_m}{\tau_m} - \sigma_{se} n_e n_m \bar{v}, \tag{2}$$

$$\frac{dT_e}{dt} = -aT_e^{1/2}(T_e - T_G) - \frac{bn_e T_e^{1/2}(T_e - T_G)}{T_e^2} + \frac{2}{3k}\sigma_{se} n_m \epsilon_m \bar{v} + H \tag{3}$$

where

n_m = metastable density
n_e = electron density
T_e = electron temperature
T_G = gas temperature
$\bar{v}$ = electron average velocity
τ_m, τ_e = metastable and electron volume loss time constants
a = proportionality factor for electron-atom collisions (constant P_c)
b = proportionality factor for electron-ion collisions (includes $\ell n\,(T_e^{3/2}/n_e^{1/2})$ factor)
$k = 1.38 \times 10^{-23}$ joules/deg. K
σ_{se} = cross section for superelastic collisions
ϵ_m = energy released in superelastic collision (~20 ev)

H = other heating phenomena.

The initial metastable density n_{mo} is given by

$$n_{mo} = \frac{\delta N_o n_{eo}}{(\delta+\sigma_{se} v_o) n_{e0} + \frac{1}{\tau_{mo}}}, \tag{4}$$

where δ is the metastable production cross section averaged over the electron distribution, and N_o is gas particle density.

If we neglect electron-ion collisions and assume only metastable heating, the asymptotic solution for the temperature when the metastable heating decreases more slowly than the electron temperature would in the absence of heating is

$$T = T_G + \frac{2\sigma_{se}\epsilon_m}{3ka} n_m ,$$

and indeed the electron temperature will decay with the metastable time constant.

When the electron density becomes appreciable, the analysis is not so straightforward. In this case the equation is rewritten

$$n_m = \frac{1}{\frac{2}{3k}\sigma_{se}\epsilon_m \bar{v}} \left[\frac{dT_e}{dt} + a T_e^{1/2}(T_e - T_G) + \frac{b n_e T_e^{1/2}(T_e - T_G)}{T_e^2} \right] \tag{5}$$

All of the quantities on the right are determined either from the temperature-decay curve or from independent measurements, and thus the metastable decay can be calculated. This decay is then compared with the decay predicted from Eq. 2. The agreement is encouraging, but the analysis is still not complete. Better measurements of n_e are awaited.

The heating resulting from $He + He^* \rightarrow He_2^+ + e^-$ should also be considered, since calculations show that it could contribute significantly to the heating. This term would have the form

$$H \propto \frac{p n^*}{n_e} ,$$

where

p = gas pressure,

n^* = density of excited helium states of sufficient energy to participate in the reaction.

Calculations at 1-mm pressure gave surprisingly good agreement between the initial metastable density calculated by Eq. 4 and the metastable density calculated from

Eq. 5 and extrapolated to time zero. This is actually an independent check on the super-elastic heating assumption, since δ of Eq. 4 does not enter into Eq. 5.

We see that the apparently correct temperature decay for the electrons observed at low pressures[4] may well have been a real observation, since there are pressures for which the asymptotic decay will be the "unheated" form rather than the "heated" form.

This is encouraging, since the heavier noble gases that will be investigated with slower energy decay times may have a larger range of pressure over which the "unheated" decay is the asymptotic form.

J. C. Ingraham

References

1. J. C. Ingraham and J. J. McCarthy, Quarterly Progress Report No. 64, Research Laboratory of Electronics, M.I.T., January 15, 1961, pp. 76-79.

2. G. Bekefi and J. L. Hirshfield, Radiation from plasmas with non-Maxwellian distributions, Quarterly Progress Report No. 59, Research Laboratory of Electronics, M.I.T., October 15, 1960, pp. 3-8.

3. A. Phelps and S. C. Brown, Phys. Rev. 86, 102 (1952).

4. At low pressures the metastable atoms diffuse rapidly to the walls and do not contribute to asymptotic heating.

C. ELECTRON ENERGIES FROM THE LANGEVIN EQUATION

Allis[1] has derived expressions for the instantaneous drift and total energies of an assembly of electrons from the Langevin equation. The case for a uniform applied magnetic field and a single component of ac electric field perpendicular to the magnetic field was solved. In this report these results have been extended to include the contributions of all three ac components plus a dc component of electric field parallel to the magnetic field.

The computation is long and tedious, principally because only the real part of the complex drift velocity must be squared to obtain the drift energy. All phase angles appear explicitly. Therefore we shall sketch only enough of the derivation to define the notation and state the results corresponding to Allis' Eqs. (12.8) and (16.4) for the drift and total energies.

The momentum and energy equations for a single electron are:

$$m\dot{\bar{v}} = -e\bar{E} + e\bar{B} \times \bar{v} + m\bar{A}(t) \tag{1}$$

$$\dot{u} = \frac{d}{dt}\left(\frac{1}{2}mv^2\right) = -e\bar{E} \cdot \bar{v} + m\bar{A}(t) \cdot \bar{v} \,. \tag{2}$$

Here, $\bar{A}(t)$ is the stochastic force caused by collisions with gas molecules. Take the time average of the stochastic terms over several collision times to be

$$\overline{m\bar{A}(t)} = -\nu_c m\bar{v}_d \tag{3}$$

$$\overline{m\bar{A}(t)\cdot\bar{v}} = -\lambda\nu_c(u-\bar{U}) , \tag{4}$$

where $\bar{v}_d$ is the instantaneous electron drift velocity, and u the instantaneous energy (assumed not to change appreciably during the time of averaging), and $\bar{U}$ is the average gas energy, ν_c is the collision frequency for momentum transfer, and λ is the energy loss parameter.

The velocity of an electron is

$$\bar{v} = \bar{v}_r + \bar{v}_d = \bar{v}_r + (\bar{v}_o+\bar{v}_{ac}) , \tag{5}$$

where $\bar{v}_r$ is the random velocity, $\bar{v}_d$ the drift velocity that splits into a steady part $\bar{v}_o$, and an alternating part $\bar{v}_{ac}$. Similarly, the energy is the sum of the random plus drift energies

$$u = u_r + u_d = \frac{1}{2} mv_r^2 + \frac{1}{2}mv_d^2 . \tag{6}$$

Taking the ensemble averages of Eqs. 1 and 2 over many electrons at time t and setting the ensemble averages of the stochastic terms equal to the time averages of Eqs. 3 and 4, we eliminate the random velocity.

$$m\dot{\bar{v}}_d = -e\bar{E} + e\bar{B}\times\bar{v}_d - \nu_c m\bar{v}_d \tag{7}$$

$$\dot{u} = -e\bar{E}\cdot\bar{v}_d - \lambda\nu_c(u-\bar{U}) . \tag{8}$$

Equation 7 can be sloved for the steady-state drift velocity, by using complex notation:

$$\bar{E}(t) = \bar{E}_o + \bar{E}_{ac}(t)$$

$$= \hat{i}_1 E_1 \exp[j(\omega t+\delta_1)] + \hat{i}_2 E_2 \exp[j(\omega t+\delta_2)] + \hat{i}_3(E_o+E_3 \exp[j(\omega t+\delta_3)])$$

$$\bar{B} = \hat{i}_3\bar{B}, \qquad \omega_b = eB/m$$

$$\bar{v}_{ac} = -\bar{\bar{\mu}}\cdot\bar{E}_{ac} = \hat{i}_1 v_1 \exp[j(\omega t+\phi_1)] + \hat{i}_2 v_2 \exp[j(\omega t+\phi_2)] + \hat{i}_3 v_3 \exp[j(\omega t+\phi_3)]$$

$$\bar{v}_o = -\mu_o\bar{E}_o = \hat{i}_3 v_o = -\hat{i}_3\mu_o E_o$$

The E_i and v_i are all real. Let $\delta = \delta_2 - \delta_1$ and $\epsilon = \frac{E_2}{E_1}$ be a measure of the ellipticity of the electric polarization in the transverse plane. Right circular polarization, which is responsible for electron resonance, occurs for $\delta = -\frac{\pi}{2}$, $\epsilon = 1$. The ac mobility tensor

has been given by Allis,[1] but we shall write it in a different form, making the phase angles explicit:

$$\bar{\bar{\mu}} = \begin{bmatrix} \mu_T e^{-j\phi_T} & -\mu_\perp e^{-j\phi_\perp} & 0 \\ \mu_\perp e^{-j\phi_\perp} & \mu_T e^{-j\phi_T} & 0 \\ 0 & 0 & \mu_\parallel e^{-j\phi_\parallel} \end{bmatrix} \tag{9}$$

where

$$\mu_T = \frac{e}{m}\frac{\Omega_o}{\Omega_r\Omega_\ell} \qquad \Omega_r^2 = \nu_c^2 + (\omega-\omega_b)^2$$

$$\mu_\perp = \frac{e}{m}\frac{\omega_b}{\Omega_r\Omega_\ell} \qquad \Omega_\ell^2 = \nu_c^2 + (\omega+\omega_b)^2$$

$$\mu_\parallel = \frac{e}{m\Omega_o} \qquad \Omega_o^2 = \nu_c^2 + \omega^2$$

$$\mu_o = \frac{e}{m\nu_c}$$

$$\tan\phi_T = \frac{\omega}{\nu_c}\frac{(\nu_c^2+\omega^2-\omega_b^2)}{(\nu_c^2+\omega^2+\omega_b^2)}$$

$$\tan\phi_\perp = \frac{\nu_c}{\omega_b}\frac{(2\omega-\omega_b)}{(\nu_c^2+\omega_b^2-\omega^2)}$$

$$\tan\phi_\parallel = \frac{\omega}{\nu_c}$$

The real drift velocity is

$$\begin{aligned}\bar{v}_d = {} & \hat{i}_1[\mu_T E_1 \cos(\omega t+\delta_1-\phi_T) - \mu_\perp E_2 \cos(\omega t+\delta_2-\phi_\perp)] \\ & + \hat{i}_2[\mu_\perp E_1 \cos(\omega t+\delta_1-\phi_\perp) + \mu_T E_2 \cos(\omega t+\delta_2-\phi_T)] \\ & + \hat{i}_3[\mu_o E_o + \mu_\parallel E_3 \cos(\omega t+\delta_3-\phi_\parallel)].\end{aligned} \tag{10}$$

The drift energy may be written

$$u_d(t) = u_o(t) + u_{ac}(t) = \frac{1}{2}m(\bar{v}_o+\bar{v}_{ac})^2 = \frac{1}{2}mv_o^2 + m\bar{v}_o \cdot \bar{v}_{ac} + \frac{1}{2}mv_{ac}^2$$

$$= \bar{u}_o + u_{o_{||}} \cos(\omega t-\phi_{||}') + \bar{u}_{ac} + u_I \cos 2(\omega t-\phi_I) + u_{||} \cos 2(\omega t-\phi_{||}'), \tag{11}$$

where

$$u_o(t) = \frac{1}{2}mv_o^2 + m\bar{v}_o \cdot \bar{v}_{ac} = \bar{u}_o + u_{o_{||}} \cos(\omega t-\phi_{||}') \tag{12a}$$

$$\bar{u}_o = \frac{1}{2}mv_o^2 = \frac{e^2}{2m\nu_c^2}E_o^2 \tag{12b}$$

$$u_{o||} = mv_o v_3 = \frac{e^2}{m}\frac{E_o E_3}{\nu_c \Omega_o} \tag{12c}$$

$$u_{ac}(t) = \frac{1}{2}mv_{ac}^2 = \bar{u}_{ac} + u_I \cos 2(\omega t-\phi_I) + u_{||} \cos 2(\omega t-\phi_{||}') \tag{12d}$$

$$\bar{u}_{ac} = \frac{e^2}{4m}\left[\frac{\frac{1}{2}\left(\Omega_r^2+\Omega_\ell^2\right)(1+\epsilon^2) - 4\omega\omega_b\epsilon\sin\delta}{\Omega_r^2\Omega_\ell^2}\right]E_1^2 + \frac{e^2E_3^2}{4m\Omega_o^2} \tag{12e}$$

$$u_I = \frac{e^2}{4m}\frac{\left[\left(\nu_c^2+\omega^2+\omega_b^2\right)^2 - 4\omega^2\omega_b^2\right]^{1/2}}{\left[\left(\nu_c^2+\omega^2-\omega_b^2\right)^2 + 4\nu_c^2\omega_b^2\right]}\left[(1+\epsilon^2)^2 - 4\epsilon^2\sin^2\delta\right]^{1/2}E_1^2 \tag{12f}$$

$$u_{||} = \frac{1}{4}mv_3^2 = \frac{e^2E_3^2}{4m\Omega_o^2} \tag{12g}$$

$$\tan 2\phi_1 = \frac{\frac{2\omega\nu_c}{\nu_c^2+\omega_b^2-\omega^2} - \frac{\epsilon^2\sin 2\delta}{1+\epsilon^2\cos 2\delta}}{1 + \frac{2\omega\nu_c}{\nu_c^2+\omega_b^2-\omega^2}\cdot\frac{\epsilon^2\sin 2\delta}{1+\epsilon^2\cos 2\delta}} \tag{12h}$$

$$\phi_{||}' = \phi_{||} - \delta_3 . \tag{12i}$$

Equations 11 and 12 reduce to Allis' Eq. (12.8) when $E_o = E_3 = \epsilon = \delta = 0$.

To integrate Eq. 8 for u(t), we must first determine the power input from $-e\bar{E} \cdot v_d$, using the real parts of E and v_d. The result is

$$-e\bar{E}(t)\cdot\bar{v}_d(t) = 2\nu_c u_d(t) - \omega m\bar{v}_{ac}\left(t-\frac{T}{4}\right)\cdot\left[\bar{v}_{ac}(t)+\bar{v}_o\right], \tag{13}$$

where $T = 2\pi/\omega$ is the period of the ac field. The second term on the right is the reactive power, stored as electron kinetic energy. The reactive power was omitted by Allis. Equation 13 is substituted in (8) and we revert to complex variables to solve

$$\dot{u} + \lambda\nu_c(u-\bar{U}) = 2\nu_c(\bar{u}_{ac}+\bar{u}_o) + 2u_I(\nu c+j\omega)\exp\left[2j(\omega t-\phi_I)\right]$$
$$+ 2u_{II}\,(\nu_c+j\omega)\exp\left[2j(\omega t-\phi_{II}')\right] + u_{o_{II}}\,(2\nu_c+j\omega)\exp\left[j(\omega t-\phi_{II}')\right] \tag{14}$$

Let $u-\bar{U} = A + B_I\exp\left[2j(\omega t-\phi_I)\right] + B_{II}\exp\left[2j(\omega t-\phi_{II}')\right] + C\exp\left[j(\omega t-\phi_{II}')\right]$ and solve for the coefficients, then

$$A = 2\frac{\bar{u}_{ac}+\bar{u}_o}{\lambda} = \frac{2\bar{u}_d}{\lambda} \tag{15a}$$

$$B_I = \frac{2u_I\,(\nu_c+j\omega)}{(\lambda\nu_c+2j\omega)} = \frac{2u_I}{\lambda}\,\frac{\left(1+\dfrac{\omega^2}{\nu_c^2}\right)^{1/2}}{\left(1+\dfrac{4\omega^2}{\lambda^2\nu_c^2}\right)^{1/2}}\,e^{-2j\psi_I} \tag{15b}$$

$$B_{II} = \frac{u_{II}}{u_I}B_I \tag{15c}$$

$$C = \frac{u_{o_{II}}\,(2\nu_c+j\omega)}{(\lambda\nu_c+j\omega)} = \frac{2u_{o_{II}}}{\lambda}\,\frac{\left(1+\dfrac{\omega^2}{4\nu_c^2}\right)}{\left(1+\dfrac{\omega^2}{\lambda^2\nu_c^2}\right)}\,e^{-j\psi_{o_{II}}} \tag{15d}$$

$$\tan 2\psi_I = \frac{\omega}{\nu_c}\,\frac{(2-\lambda)}{\left(\lambda+\dfrac{2\omega^2}{\nu_c^2}\right)} \approx \frac{2\omega}{\nu_c}\,\frac{1}{\left(\lambda+\dfrac{2\omega^2}{\nu_c^2}\right)} \tag{15e}$$

$$\tan\psi_{o_{II}} = \frac{\omega}{2\nu_c}\,\frac{(2-\lambda)}{\left(\lambda+\dfrac{\omega^2}{2\nu_c^2}\right)} \approx \frac{\omega}{\nu_c}\,\frac{1}{\left(\lambda+\dfrac{\omega^2}{2\nu_c^2}\right)}. \tag{15f}$$

Finally, we express the real energy in the form of Allis' Eq. (16.4) as

$$u - \bar{u} = \frac{2\bar{u}_d}{\lambda} \left\{ 1 + \frac{a_I \cos 2(\omega t - \phi_I - \psi_I) + a_{II} \cos 2(\omega t - \phi_{II}' - \psi_{II})}{\sqrt{\left(1 + \frac{4\omega^2}{\lambda^2 \nu_c^2}\right) \Big/ \left(1 + \frac{\omega^2}{\nu_c^2}\right)}} \right.$$

$$\left. + \frac{a_{O\,II} \cos (\omega t - \phi_{II}' - \psi_{O\,II})}{\sqrt{\left(1 + \frac{\omega^2}{\lambda^2 \nu_c^2}\right) \Big/ \left(1 + \frac{\omega^2}{4\nu_c^2}\right)}} \right\} \qquad (16)$$

where $a_I = \frac{u_I}{\bar{u}_d}$, $a_{II} = \frac{u_{II}}{\bar{u}_d}$, and $a_{O\,II} = \frac{u_{O\,II}}{\bar{u}_d}$. Equation 16 reduces to Allis' Eq. (16.4), when $E_o = E_3 = \epsilon = \delta = 0$ and the reactive power is omitted. Reactive power can be neglected in (15) and (16) by neglecting ω/ν_c as compared with 1 but not $\omega/\lambda\nu_c$, regardless of the actual value of ω/ν_c.

C. D. Buntschuh

References

1. W. P. Allis, Motions of Ions and Electrons, Technical Report 299, Research Laboratory of Electronics, M. I. T., June 13, 1956.

D. HARMONICS OF ELECTRON-CYCLOTRON EMISSION FROM LOW AND INTERMEDIATE PRESSURE DISCHARGES

An increase in the radiation at the electron-cyclotron harmonic frequencies has been observed in the microwave emission from the positive column of a low-pressure, high-current, mercury-vapor discharge immersed in a magnetic field,[1] in which the degree of ionization was less than 0.1 per cent. Similar emissions have been observed in intermediate pressure argon and helium discharges of low ionization and in a low-pressure fully ionized argon arc.

The discharge experiments at the intermediate pressures were performed with the same equipment used in the earlier low-pressure mercury experiments. The plasma frequency was greater than or equal to the measuring frequency. The collision frequency was estimated to be in the range $0.02 \leq \nu/\omega \leq 0.2$. The amplitudes and shapes of the harmonics were studied in argon as functions of discharge currents, pressure, and measuring frequency.

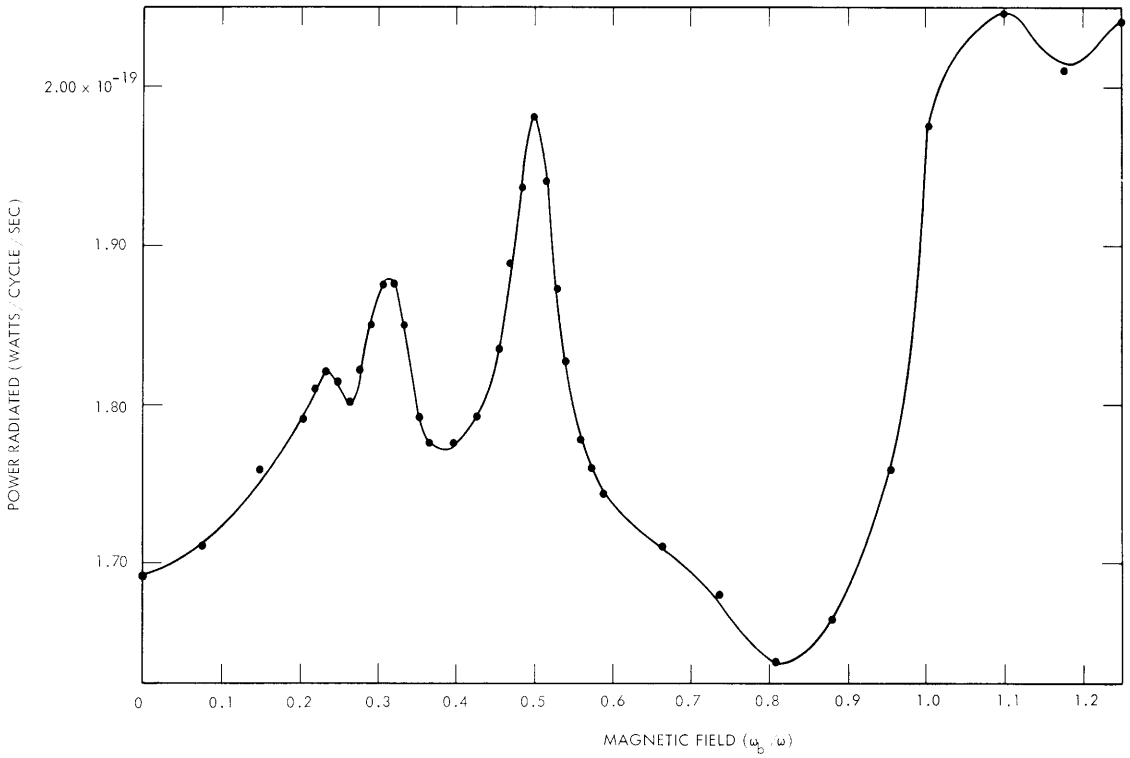

Fig. X-1. Power radiated from the positive column as a function of the axial magnetic field. Discharge current, 1 amp; argon pressure in discharge, 0.6 mm Hg; measuring frequency, 2980 mc.

Under suitable conditions (see below), three or four harmonics other than the first or fundamental were observed. The amplitude of successive harmonics decreased until the higher harmonics were not distinguishable from the background emission. (See Fig. X-1.)

The low-pressure argon arc experiments were conducted with the vacuum arc facility. In these experiments, the arc current was varied from 3.5 amps to 20 amps. The argon gas pressure was held constant at several microns of mercury. The ratio of the collision frequency to the observation frequency, ω, was approximately 5×10^{-4}. The magnetic field was varied from 95 gauss to 1500 gauss. An X-band radiometer was employed to measure the radiation at 9000 mc within a narrow frequency band 8 mc wide. An X-band horn received the radiation from a four-inch length of the arc. The horn was oriented to receive radiation propagating at right angles to the applied magnetic field.

The second through the tenth harmonics were observed in the arc experiments. The magnetic field could not be increased sufficiently to observe the first or fundamental harmonic. The amplitudes of the harmonics relative to the background emission do not

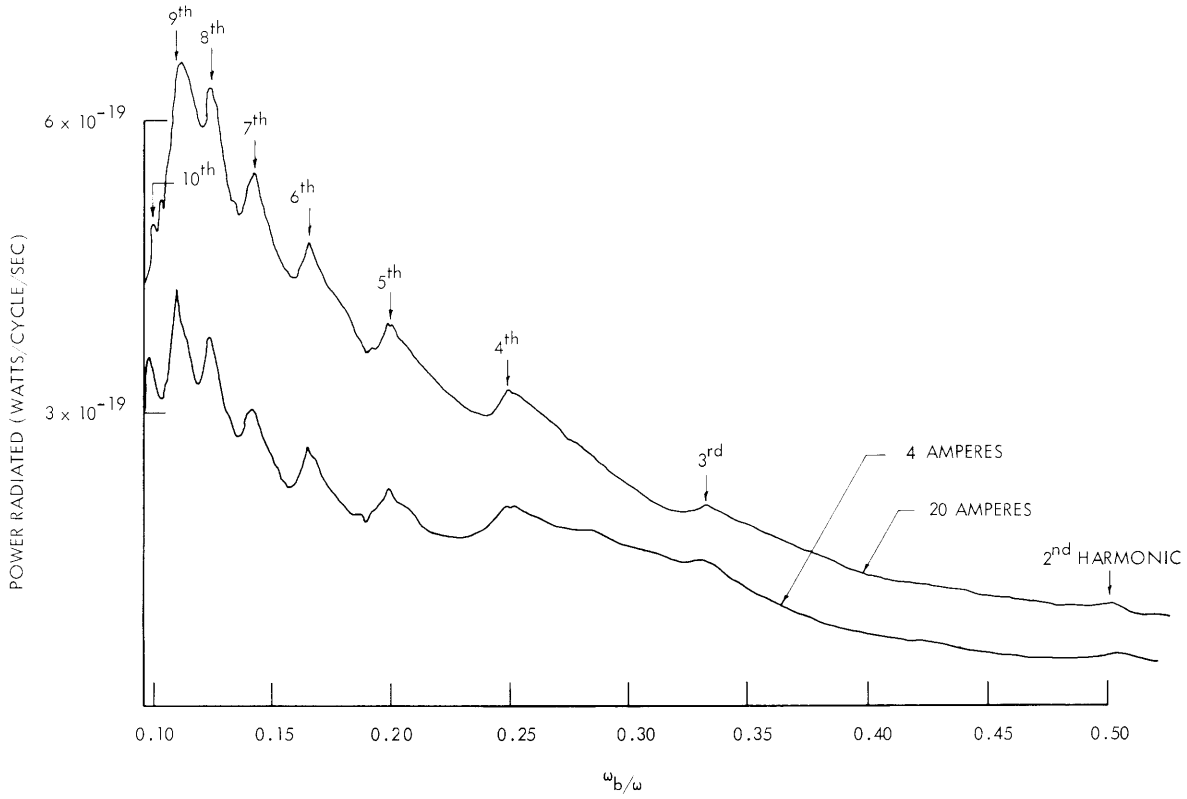

Fig. X-2. Power radiated from a 4-inch section of the argon arc as a function of the axial magnetic field at arc currents of 4 and 20 amps, argon pressure 2 microns of Hg, and a measuring frequency of 9037 mc/s.

decrease with increasing harmonic number. In most cases the second and third harmonics are less pronounced than the higher harmonics. (See Fig. X-2.)

1. Dependence on Discharge Current

In the intermediate-pressure experiments the harmonics appear at discharge currents of 0.4-0.6 amperes. The amplitude of the harmonics remains approximately constant for currents in the range 0.7-1.0 amps; no measurements could be made at higher currents.

In the arc experiments, the amplitudes of the harmonics were approximately constant over the range 4.0-20.0 amperes. Figure X-2 shows the emission at 4 amps and at 20 amperes. The background emission is greater for an arc current of 20 amps than for a current of 4 amps because of the larger electron temperature at higher currents.

It appears in both the intermediate-pressure experiments and the arc experiments that once the electron density is high enough, the harmonics are not strongly dependent on the density.

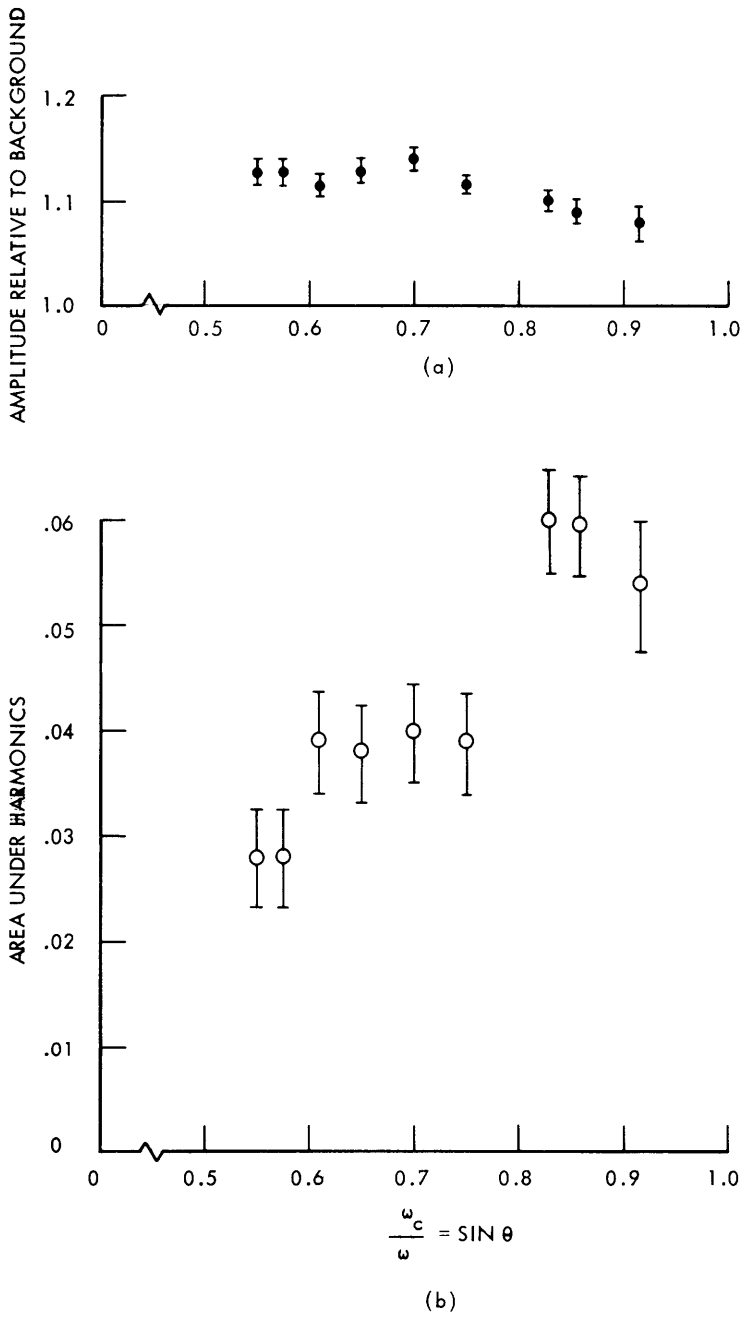

Fig. X-3. Characteristics of the second harmonic as a function of measuring frequency. The angle of propagation is $\theta = \sin^{-1} \omega_c/\omega$; discharge current, 1 amp; discharge pressure, 0.6 mm Hg in argon. (a) Amplitude of second harmonic relative to the background, P_2/P_o. (b) Relative area under harmonic, estimated as $\Delta \cdot (P_2/P_o)$. Δ is the width of the harmonic at 3/4 amplitude.

2. Pressure Dependence in the Intermediate-Pressure Discharges

The amplitude and shape of the harmonics was found to be independent of pressure in the range 0.3-0.8 mm Hg. The electron-neutral collision frequency has been estimated to vary by a factor of two in this region, so that the peaks are not predominantly pressure-broadened.

As the pressure is increased to 2 mm Hg, the harmonics decrease in amplitude and disappear into the background. The widths of the peaks remain about the same as in the lower pressure region.

At pressures below ~ 0.3 mm Hg, the harmonics are obscured by an increase in the background radiation.

3. Frequency Dependence in the Intermediate-Pressure Discharges

The amplitudes and shapes of the harmonics were also studied as a function of the measuring frequency. Because the plasma is in a waveguide, the angle of propagation of the radiation relative to the waveguide axis (and hence the magnetic field) changes with the frequency. If ω_c is the cutoff frequency of the waveguide, the angle of propagation is $\theta = \sin^{-1} \omega_c/\omega$.

In these experiments the ratio of the plasma frequency to the measuring frequency changes. It is believed, however, that the observed changes in the characteristics of the harmonics are primarily due to the change in angle of propagation. The frequency was varied between 2300 mc and 3800 mc, corresponding to angles of propagation between between 65° and 33°.

We found that the amplitude of a given harmonic remained approximately constant relative to the background amplitude. That is, the amplitude of the harmonic divided by the amplitude of the background is roughly independent of the measuring frequency. (See Fig. X-3a.)

For frequencies above 3500 mc, the amplitude of the background drops. The plasma is considered to become transparent in this region. In the frequency region studied, the power drops by a factor of two, but the amplitude of a given harmonic relative to the background is still about the same as in the lower frequency region.

We also found that as the frequency was lowered (and the angle of propagation increased), the peaks broadened, so that the power in a given peak increased relative to the background. (See Fig. X-3b.)

4. Increased Background

For magnetic fields higher than some critical field, the background radiation from the plasma was found to increase. In the intermediate-pressure experiments this increase amounted to approximately 20 per cent. In the low-pressure arc experiments this increase was from 20 to 100 per cent in different cases. The transition from the

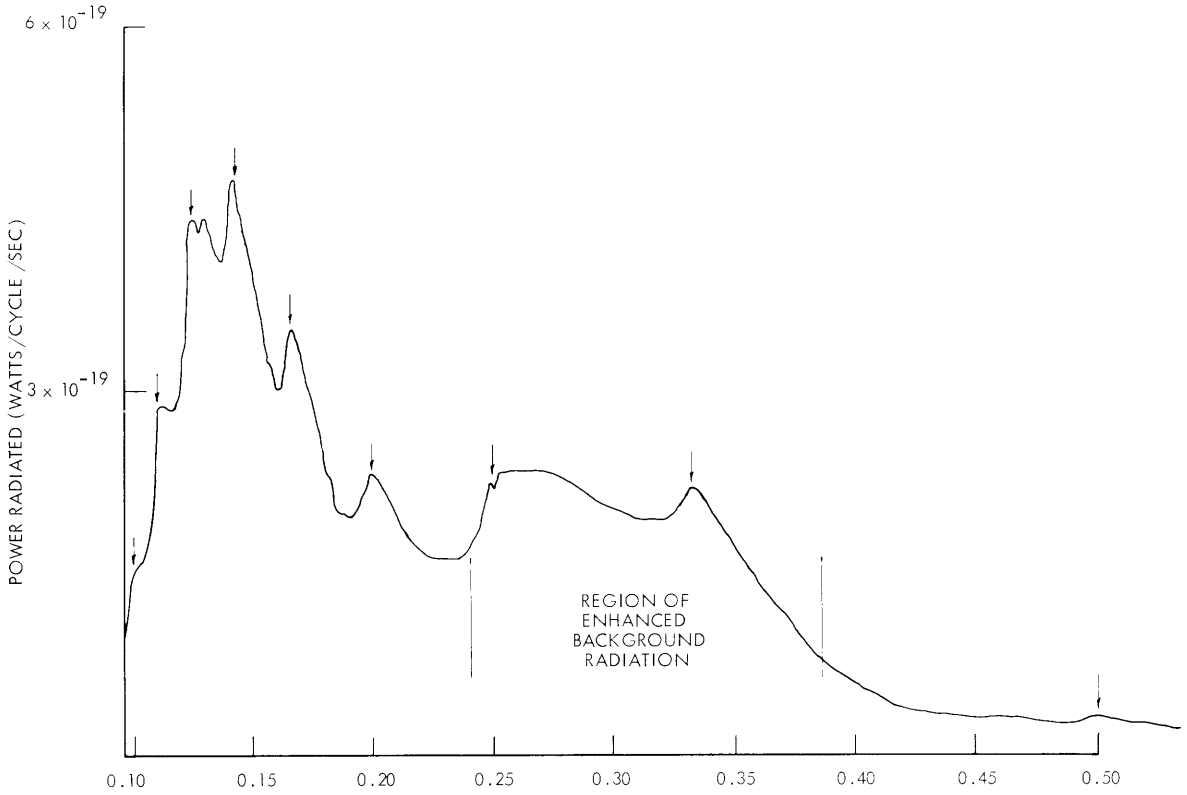

Fig. X-4. Power radiated from a 4-inch section of the argon arc as a function of the axial magnetic field, showing a region of increased background radiation and an increased third harmonic. Arc current, 5.5 amps; argon pressure, 2 μ Hg; measuring frequency, 9037 mc.

normal background to this increased background occurs very rapidly within a magnetic field change of approximately 3 per cent.

When the pressure in a 1-amp argon discharge is lowered to approximately 0.3 mm Hg, this transition occurs in the vicinity of the second harmonic. For lower pressures, the harmonics are obscured by the increase in background, although apparently still present.

We found that if the pressure was increased at a constant discharge current, the transition moved to higher magnetic fields. When the pressure is held constant and the discharge current decreased, the transition again moves to higher magnetic fields. Since in the first case the electron density is increased and the electron temperature is lowered, the increased background radiation appears to depend on the electron temperature rather than on the electron density.

Figure X-4 shows the increase in the background radiation from the argon arc operating at 5.5 amperes. This occurs over a range of magnetic fields spanning the third and fourth harmonics.

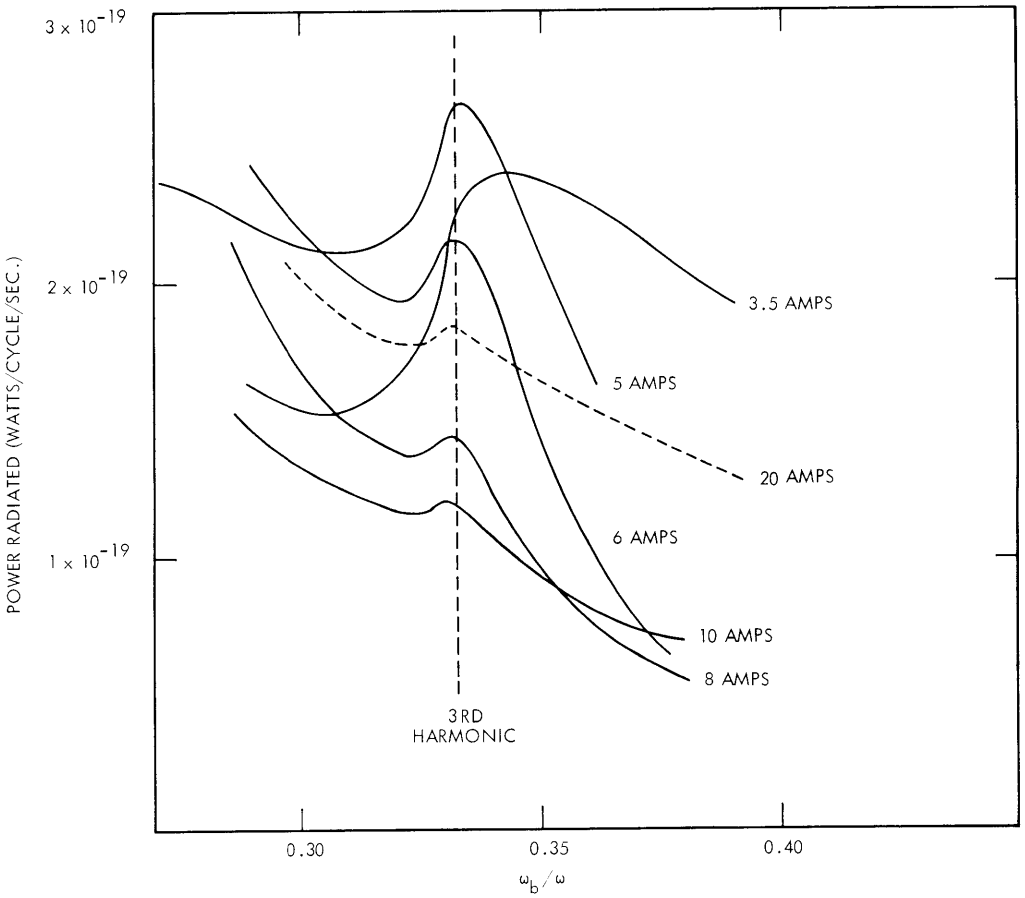

Fig. X-5. Power radiated from a 4-inch section of argon arc at the third harmonic of the electron cyclotron frequency for various values of arc current. Argon pressure, 2 μ Hg; measuring frequency, 9037 mc.

Figure X-5 shows the power radiated at the third harmonic at various values of arc current, from 3.5 to 20 amperes. At 3.5 amps the increase in the background radiation obscures the third harmonic. At 5 amps the transition region has moved to lower magnetic fields (higher harmonic number at fixed measuring frequency) and the situation is as previously shown in Fig. X-4. As the arc current is further increased, the background returns to normal. It is interesting to note that the size of the harmonic is much greater in the increased background region than in the normal background region.

The harmonics are still not understood. We may, however, rule out several possibilities.

The electron energy is too low for the harmonics to arise from relativistic electron velocities.

At the intermediate pressures, the electron drift velocity is small compared with the random velocity, and the distribution function must be almost isotropic. The harmonics are therefore not due to instabilities arising from anisotropic electron pressure, nor from an interaction between fast electrons and the plasma.

The voltage-current characteristics of the plasma indicate that we are outside the Lehnert-Kadomtsev instability.[2, 3]

The electron distribution function has not been measured in the argon discharges, but measurements in the mercury discharges used in the earlier experiments[1] indicate that it is non-Maxwellian. Measurements are planned for the study of the harmonics in the afterglow of a pulsed discharge, in which the distribution will rapidly approach Maxwellian.

E. B. Hooper, Jr., J. D. Coccoli, G. Bekefi

References

1. G. Bekefi and J. D. Coccoli, Quarterly Progress Report No. 64, Research Laboratory of Electronics, M. I. T., January 15, 1962, pp. 70-72.

2. F. C. Hoh and B. Lehnert, Phys. Fluids 3, 600 (1960).

3. B. B. Kadomtsev and A. V. Nedospasov, J. Nuclear Energy C1, 230 (1960).

E. ONE-MEGACYCLE BRIDGE FOR PLASMA MEASUREMENTS

A 1-mc bridge capable of measuring plasma conductivity has previously been reported.[1] The bridge is used in measuring the impedance of a coil with a cylindrical plasma column coaxially located, and has a sensitivity of better than 1 part in 10^8. Periodic attempts were made to correlate bridge measurements with theoretical predictions and the results were always negative. A recent review of the problem indicated that the trouble was connected with the means in which the rf fields of the coil were coupled to the plasma.

The coil is wound with 36 turns on a bobbin that is 3 5/8 inches diameter and 10 inches long. The intent of the physical arrangement is to couple the 1-mc solenoidal E_θ field to the plasma column from which one can predict the interaction. The conservative electric field of the coil, however, can be comparable to the solenoidal field, and careful shielding techniques must be used. In effect, the shields must completely eliminate capacitive coupling of the coil to the plasma but retain the inductive coupling. The previous scheme of having axial brass strips located between the coil and the plasma and properly grounded was insufficient to completely eliminate the capacitive coupling.

The scheme that has now been adopted is to use a thin conducting cylinder coaxial with and between the coil and the plasma column. This cylinder will act as a perfect electrostatic shield, and will not perturb the magnetic field as long as the skin-depth

at 1 mc is large compared with the thickness of the cylinder wall. The shield was made by painting a glass cylinder with an Aquadag solution and increasing the thickness of the layer until the desired results were obtained. An additional scheme was used to increase the axial conductivity of the cylinder over that of the azimuthal conductivity by imbedding thin axial aluminum strips in the Aquadag paint. Grounding one end of the cylinder thus insured that the whole cylinder was at rf ground potential.

Preliminary measurements were made on the positive column of a dc discharge,

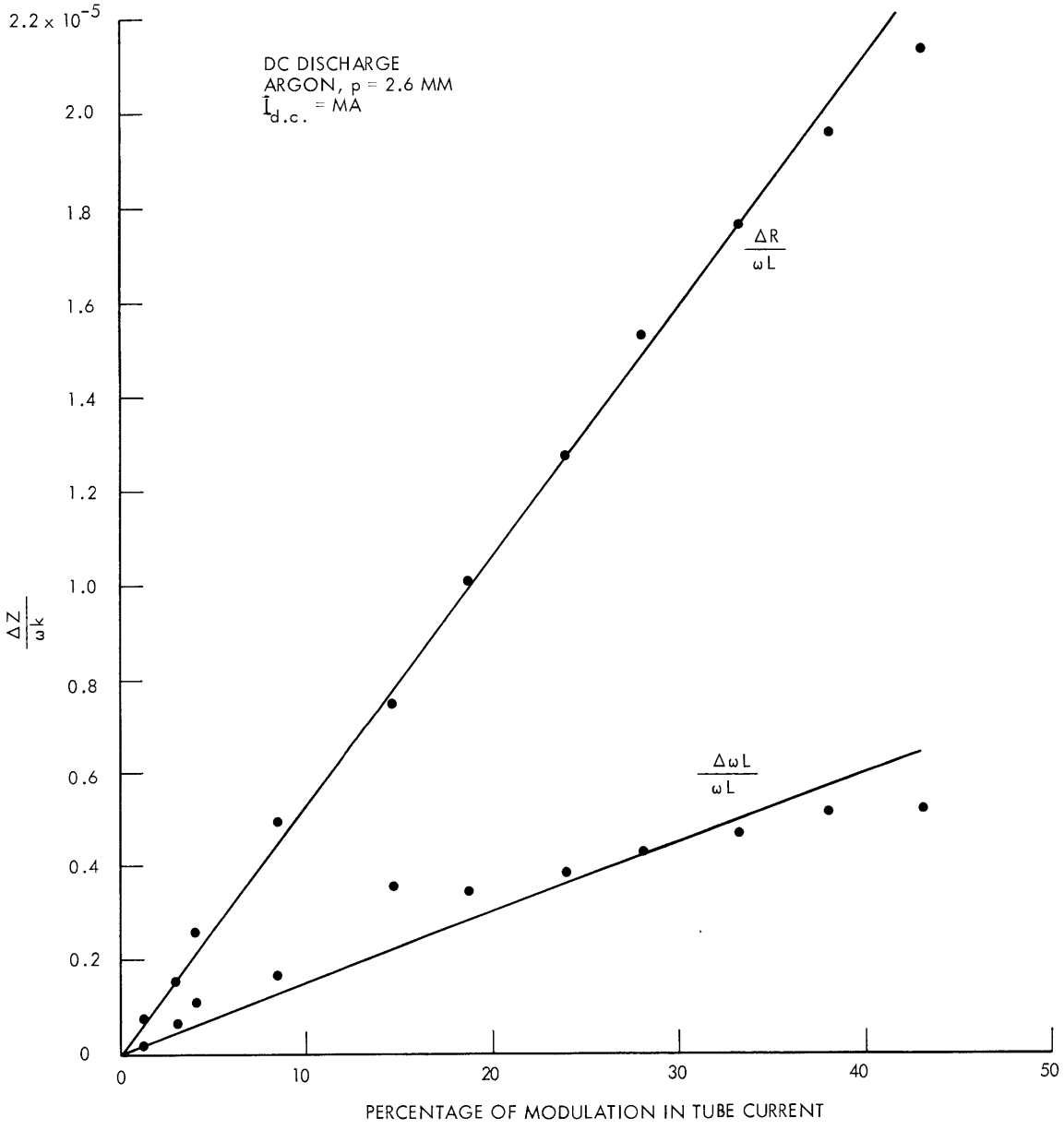

Fig. X-6. Impedance changes measured on 1-mc bridge.

1.5 inches in diameter, and at a neutral pressure of argon at 2.6 mm Hg. If one assumes that the radial dependence of the plasma density is a zero-order Bessel function, the effective change in the resistance of the coil caused by the presence of the plasma is given by

$$\Delta R = 0.104\ \epsilon_o\, \omega_p^2\, L_p\, R_p^4\, \frac{\omega^2 \nu_c^2}{\nu_c^2 + \omega^2} \left| \frac{B_{rf}}{I_{rf}} \right|^2 .$$

Here, the constant (0.104) is obtained by averaging the density distribution over the field distribution, ω_p^2 is the plasma frequency on the axis of the column, L_p and R_p are the length and radius of the plasma within the coil, ν_c is the collision frequency, and B_{rf}/I_{rf} is the ratio of the rf magnetic field inside the coil to the rf current in the coil. The change in reactance is given by a similar formula, so that $\Delta X/\Delta R = \omega/\nu_c$.

The bridge can measure small changes in impedance by virtue of modulating the unknown quantity at 100 cps and using synchronous detection. Figure X-6 shows a plot of ΔR and ΔX normalized to ωL as a function of the percentage of modulation of the tube current. The resistive part of the impedance change is seen to be sensibly linear, and its slope is amazingly so within 25 per cent of the predicted value. The reactive part of the impedance change, however, is too large and quite erratic. The ratio ω/ν_c is approximately 1000 and hence the plasma is practically all resistive. The nature of the bridge circuit does mix up real and reactive impedance changes by rotating the measured impedance by an angle θ_b, called the bridge angle. From the data, the angle appears to be around 18°, but calculations show it should be around 7°. This discrepancy is still unaccounted for. The erratic behavior of the ΔX curve can be accounted for, since small changes in the phase of the modulation cause a small fraction of the relatively large resistive change to read in the reactive channel.

With the operation of the shielding techniques thus confirmed, we are now proceeding with measurements on a plasma in a magnetic field near ion-cyclotron resonance.

D. R. Whitehouse, P. J. Freyheit

References

1. J. W. Graham and R. S. Badessa, Quarterly Progress Report, Research Laboratory of Electronics, M.I.T., April 15, 1958, p. 7.

F. DISPERSION RELATION FOR LONGITUDINAL PLASMA WAVES

The relations from which we shall start are Maxwell's curl equations and the zero and first moments of the Boltzmann equation, or the continuity and momentum equations.

$$\nabla \times \vec{E} = -\partial \vec{B}/\partial t \tag{1}$$

$$\nabla \times \vec{B} = \mu_o \vec{J} + \frac{1}{c^2}\, \partial \vec{E}/\partial t; \qquad \vec{J} = e(\vec{\Gamma}_+ - \vec{\Gamma}_-) \tag{2}$$

$$\partial N/\partial t + \nabla \cdot \vec{\Gamma} = 0 \tag{3}$$

$$\partial \vec{\Gamma}/\partial t + \frac{1}{m} \nabla \cdot \vec{\vec{P}} \pm \frac{e}{m} \left[N\vec{E} + \vec{\Gamma} \times \vec{B}\right] = 0. \tag{4}$$

Here, the plus sign refers to electrons and the minus, to ions; $\vec{\Gamma}$ is the particle flux; and N is the particle density. Equation 4 will be linearized by taking $\vec{\Gamma} \times \vec{B} = \vec{\Gamma} \times \vec{B}_o$, where B_o is the constant applied magnetic field, and $N\vec{E} = N_o\vec{E}$, with N_o the undisturbed (constant) particle density. For our purposes, it is sufficient to set $P = NKT\,\vec{\vec{I}}$ and to hold T constant. Under adiabatic conditions, the contribution of this pressure term will be changed only by a factor of γ, which is the ratio of specific heats.

All quantities are now allowed to vary as $e^{j(\omega t - \vec{k}\cdot\vec{r})}$; for example, $\vec{\Gamma}(\vec{r}, t) = \vec{\Gamma}\, e^{j(\omega t - \vec{k}\cdot\vec{r})}$, $N(\vec{r}, t) = N_o + N_1\, e^{j(\omega t - \vec{k}\cdot\vec{r})}$. By using these quantities, Maxwell's curl equations become

$$\vec{k} \times \vec{E} = \omega\vec{B} = ck_o\vec{B}, \tag{5}$$

where $k_o = \omega/c$ is the free-space wave number.

$$-j\vec{k} \times \vec{B} = \mu_o\vec{J} + j\,\omega/c^2\,\vec{E} \tag{6}$$

or, with $\mu_o = 1/\epsilon_o c^2$,

$$\vec{k}/k_o \times c\vec{B} + \vec{J}/j\epsilon_o\omega + \vec{E} = 0. \tag{7}$$

The equation of continuity now becomes

$$\omega N_1 = \vec{k} \cdot \vec{\Gamma} \tag{8}$$

or

$$k_o c N_1 = k \cdot \vec{\Gamma}. \tag{9}$$

The momentum equation is given by

$$j\omega\vec{\Gamma} - jkN_1\, kT/m \pm e/m\, (N_o E + \Gamma \times B_o) = 0 \tag{10}$$

or

$$\vec{\Gamma} - \frac{\vec{k}}{\omega}\, N_1 kT/m \pm j\, e\vec{B}_o/m\omega \times \vec{\Gamma} = \pm j\, eN_o/m\omega\, \vec{E}. \tag{11}$$

We now define: $\mp e\vec{B}_o/m = \vec{\omega}_{B_\mp}$, $\vec{\omega}_{B_\mp}/\omega = \vec{\beta}_\mp$, and rewrite the pressure term on the

left-hand side of (11) as

$$\vec{k}/\omega\ N_1 kT/m = \vec{k}/k_o\ N_1 c\ kT/mc^2 = \vec{k}/k_o\ N_1 c\delta,$$

where $\delta = kT/mc^2$. Equation 11 now becomes

$$\Gamma - \delta N_1 c\ \vec{k}/k_o - j\vec{\beta}_{\mp} \times \vec{\Gamma} = \pm j\ eN_o\vec{E}/m\omega. \tag{12}$$

It is convenient to rewrite the basic equations (5), (7), (9), and (12) in terms of a vector refractive index, $\vec{n} = \vec{k}/k_o$. With this substitution, they become

$$\vec{n} \times \vec{E} = c\vec{B} \tag{13}$$

$$\vec{n} \times c\vec{B} + \frac{\vec{J}}{j\epsilon_o\omega} + \vec{E} = 0 \tag{14}$$

$$cN_1 = \vec{n} \cdot \vec{\Gamma} \tag{15}$$

$$\vec{\Gamma} - \delta N_1 c\vec{n} - j\vec{\beta}_{\mp} \times \vec{\Gamma} = \pm j\ \frac{eN_o\vec{E}}{m\omega}. \tag{16}$$

The elimination of the perturbation density N_1 between Eqs. 15 and 16 yields

$$\vec{\Gamma} - \vec{n}(n\cdot\vec{\Gamma})\,\delta - j\vec{\beta}_{\mp} \times \vec{\Gamma} = \pm j\ \frac{eN_o\vec{E}}{m\omega}. \tag{17}$$

Equation 17 can be written in a more useful form by setting $\vec{J}_{\pm} = \pm e\vec{\Gamma}_{\pm}$ and $\epsilon_o\dot{\vec{E}} = j\omega\epsilon_o\vec{E}$ and by defining $\frac{e^2N_o}{\epsilon_o m} = \omega_p^2$ and $\omega_p^2/\omega^2 = a^2$

Finally, we have the momentum equation in the following form:

$$\vec{J}_{\mp} - \vec{n}(\vec{n}\cdot\vec{J}_{\mp})\,\delta - j\vec{\beta}_{\mp} \times \vec{J}_{\mp} = -a^2\epsilon_o\dot{\vec{E}}. \tag{18}$$

Since Eq. 18 has the same form for ions and electrons, the ± subscripts will not be included in our discussion.

Eliminating $\vec{B}$ in Maxwell's curl equations, Eqs. 13 and 14, yields the wave equation for $\vec{E}$.

$$(\vec{n}\cdot\epsilon_o\vec{E})\,\vec{n} + (1-n^2)\,\epsilon_o\vec{E} + (\vec{J}_+ + \vec{J}_-) = 0. \tag{19}$$

The momentum equation and the wave equation, Eqs. 18 and 19, are now separated into components along the k vector (indicated by subscript k) and transverse to the k vector (indicated by subscript t). The axes for the transverse components are chosen in the directions of $\vec{\beta}_t$ and $\vec{\beta}_k \times \vec{\beta}_t$. The unit vectors in these directions are designated $\hat{\ell}$ and $\hat{m}$, respectively. Note that $\beta_t = \beta \sin\theta$ and $\beta_k = \beta \cos\theta$ (see Fig. X-7).

In Eq. 18 the $\vec{\beta} \times \vec{J}$ term becomes

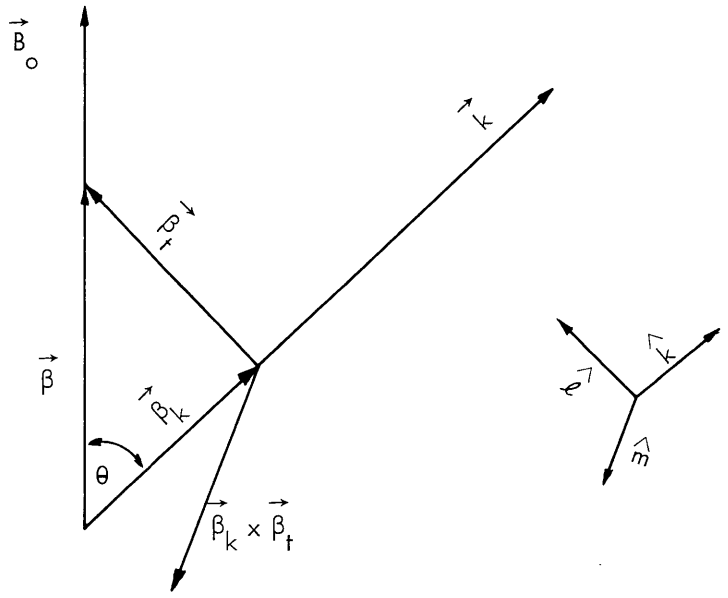

Fig. X-7. Coordinate system.

$$\hat{\beta} \times \hat{J} = (\beta_k \hat{k} + \beta_t \hat{\ell}) \times (J_k \hat{k} + J_\ell \hat{\ell} + J_m \hat{m})$$

$$= \beta_t J_m \hat{k} - \beta_k J_m \hat{\ell} + (\beta_k J_\ell - \beta_t J_k)\, \hat{m}. \tag{20}$$

In component form the momentum equation becomes

$$J_k - j\beta_t J_m - n^2 \delta J_k = -a^2 \epsilon_o \dot{E}_k \tag{21a}$$

$$J_\ell + j\beta_k J_m = -a^2 \epsilon_o \dot{E}_\ell \tag{21b}$$

$$J_m - j(\beta_k J_\ell - \beta_t J_k) = -a^2 \epsilon_o \dot{E}_m \tag{21c}$$

The wave equation (19) becomes

$$\epsilon_o \dot{E}_k + (J_+ + J_-)_k = 0 \tag{22a}$$

$$(1-n^2)\, \epsilon_o \dot{\hat{E}}_t + (\hat{J}_+ + \hat{J}_-)_t = 0 \tag{22b}$$

Note that Eq. 22a, with which we shall obtain our dispersion relation, is the charge-conservation equation: $\nabla \cdot \vec{J} + \partial\rho/\partial t = 0$. This follows from Maxwell's equations, or from the particle continuity equations. In the latter case, substitution of Poisson's equation gives $\nabla \cdot (\epsilon_o\, \partial \vec{E}/\partial t + \vec{J}) = 0$, which is (22a). Because of this, in the approximation that follows, the only Maxwell equation that we shall use is Poisson's equation.

The electromagnetic waves are eliminated by letting $c^2 \to \infty$. Since this approximation implies that $n^2 = c^2/u^2 \to \infty$, where u is the phase velocity, Eq. 22b shows that the transverse fields vanish, $\bar{\bar{E}}_t \to 0$. This can therefore be called the "longitudinal approximation." Conversely, the longitudinal waves, called plasma waves, would be eliminated by neglecting the pressure term $n^2 \delta J_k$ in Eq. 21a, which implies that $u^2 \gg V_T^2$, where $V_T = (KT/m)^{1/2}$ is the thermal velocity.

With the aid of the longitudinal approximation, (21b) and (21c) can be solved for J_m in terms of J_k. The resulting relation is

$$J_m\left(1-\beta_k^2\right) = -j\beta_t J_k. \tag{23}$$

Substitution of Eq. 23 in (21a) gives

$$J_k(1-\delta n^2) - \beta_t^2/1-\beta_k^2\, J_k = -a^2 \epsilon_o \dot{E}_k \tag{24}$$

or

$$J_k\left[\left(1-\beta^2\right) - n^2\delta\left(1-\beta_k^2\right)\right] = -a^2\left(1-\beta_k^2\right)\epsilon_o \dot{E}_k. \tag{25}$$

The charge-conservation equation, (22a), then becomes

$$\epsilon_o \dot{E}_k \left\{ 1 - \frac{a_+^2\left(1-\beta_+^2\cos^2\theta\right)}{\left[\left(1-\beta_+^2\right) - n^2\delta_+\left(1-\beta_+^2\cos^2\theta\right)\right]} - \frac{a_-^2\left(1-\beta_-^2\cos^2\theta\right)}{\left[\left(1-\beta_-^2\right) - n^2\delta_-\left(1-\beta_-^2\cos^2\theta\right)\right]} \right\} = 0. \tag{26}$$

For $E_k \neq 0$ and with the convenient substitutions, $a^2/\delta = A$ and $(1-\beta^2)/\delta(1-\beta^2\cos^2\theta) = B$, the dispersion relation is

$$\frac{A_+}{B_+ - n^2} + \frac{A_-}{B_- - n^2} = 1, \tag{27}$$

and the particle-flux equations take the form:

$$e\Gamma_k^-/\epsilon_o \dot{E}_k = -J_k^-/\epsilon_o \dot{E}_k = A_-/B_- - n^2 \tag{28a}$$

$$e\Gamma_k^+/\epsilon_o \dot{E}_k = J_k^+/\epsilon_o \dot{E}_k = -A_+/B_+ - n^2. \tag{28b}$$

Equation 27 has two solutions for n^2 which are referred to as the plasma-electron and plasma-ion waves. It is desirable to have a criterion by which these names can be properly ascribed to the two waves, and such a criterion exists in the phase relation between the currents J_+ and J_-. The currents are in phase for one solution and out of phase for the other.

This relation can be easily demonstrated. The ratio of the electron and ion particle flux is

$$\Gamma_-/\Gamma_+ = -\left(A_-/B_- - n^2\right)\left(B_+ - n^2/A^+\right), \tag{29}$$

or, by use of the dispersion relation,

$$\Gamma_-/\Gamma_+ = \frac{n^2 - (B_+ - A_+)}{A_+}. \tag{30}$$

The dispersion relation, when written as a quadratic in n^2, is

$$n^4 - n^2\left[(B_+ - A_+) + (B_- - A_-)\right] + (B_+ - A_+)(B_- - A_-) - A_+A_- = 0. \tag{31}$$

The two solutions for n^2 are designated n_1^2 and n_2^2. Therefore, the product of the flux ratios for the two solutions is

$$(\Gamma_-/\Gamma_+)_1\,(\Gamma_-/\Gamma_+)_2 = 1/A_+\left[n_1^2\,n_2^2 - (B_+ - A_+)\left(n_1^2 + n_2^2\right) + (B_+ - A_+)^2\right]. \tag{32}$$

Using the values of $n_1^2 n_2^2$ and $n_1^2 + n_2^2$ from the coefficients of Eq. 31, we find that

$$(\Gamma_-/\Gamma_+)_1\,(\Gamma_-/\Gamma_+)_2 = -A_-/A_+ = -T_+/T_-. \tag{33}$$

Therefore, when the particles or currents are in phase for one wave, they are out of phase for the other. We call the plasma-electron wave the one for which the currents are in phase and therefore the electrons and ions move in opposite directions. The plasma-ion wave then has the opposite property, electrons and ions moving together as they would in a sound wave. Equation 28 is used to determine this phase relationship.

The accompanying figure (Fig. X-8) shows the a^2, β^2 plane divided into various regions as described below. In each region a schematic polar plot of the phase velocity of the longitudinal waves is shown. The following definitions are used. $a_\pm^2 = \frac{N_o e^2}{\epsilon_o \omega^2 m_\pm} = \frac{\omega_{p\pm}^2}{\omega^2}$, where ω_p = plasma frequency, $a^2 = a_+^2 + a_-^2$ and; $\beta_\pm = \frac{eB_o}{m \pm \omega} = \omega_{b\pm}/\omega$, where ω_b = cyclotron frequency. The resonance angles are $\theta_R^\pm$, the angles at which the phase velocity goes to zero. They are determined by the equation

$$\tan^2 \theta_R^\pm = \beta_\pm^2 - 1. \tag{34}$$

The cutoff angle is θ_e, the angle at which the phase velocity becomes infinite. For this

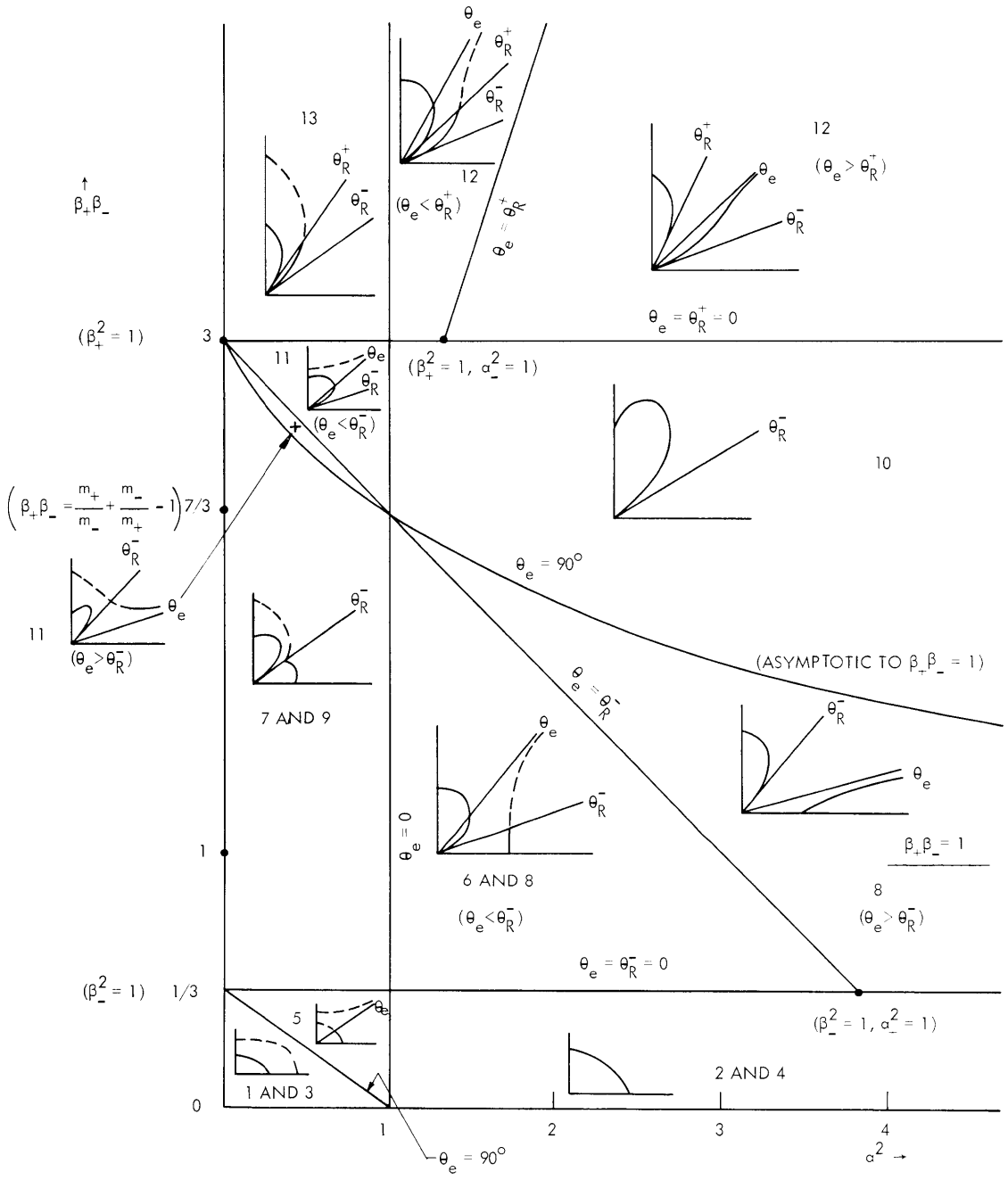

Fig. X-8. Polar phase velocity plots of longitudinal plasma waves in the α^2, β^2 plane.

angle the longitudinal waves couple to the electromagnetic waves. This angle is defined by the relation

$$\tan^2 \theta_e = \frac{(a^2-1)\left(\beta_+^2-1\right)\left(\beta_-^2-1\right)}{\left(1-\beta_-^2\right)\left(1-\beta_+^2\right) - a^2(1-\beta_+\beta_-)} . \tag{35}$$

The regions of the a^2, β^2 plane are designated by the commonly used numerical notation. The longitudinal waves are uncoupled from the electromagnetic waves in regions (1, 3), (2, 4), (7, 9), (10), and (13), and coupling is present in regions (5), (6, 8), (11), and (12). The following equations determine these regions.

The straight lines:

$a^2 = 1$, $\beta_+^2 = 1$, $\beta_-^2 = 1$

$\beta_+\beta_- = m_+/m_- - a^2(1-m_-/m_+)$, which subdivides regions (6, 8) and (11)

$\beta_+\beta_- = m_-/m_+ - a^2(1-m_+/m_-)$, which subdivides region (12)

The hyperbola:

$$\left(1-\beta_-^2\right)\left(1-\beta_+^2\right) - a^2(1-\beta_+\beta_-) = 0 .$$

In the polar plots the vertical line ($\theta=0$) is in the direction of the constant magnetic field; the horizontal line ($\theta=\pi/2$) is at right angles to the field. Only one quadrant is shown. The complete phase velocity surface is obtained by reflection about $\theta = \pi/2$ and rotation about $\theta = 0$. Solid curves indicate that $\Gamma_k^-/\Gamma_k^+ > 0$, that is, ions and electrons in phase; and dashed curves indicate that $\Gamma_k^-/\Gamma_k^+ < 0$, that is, ions and electrons out of phase. In order to improve resolution, the ratios $T_-/T_+ = 2$ and $m_+/m_- = 3$ were used in the computations.

H. R. Radoski

G. COMMENTS ON PLASMA CONSTRICTION

In a previous report[1] Magda Erickson developed from thermodynamic principles a theory to explain an observed constriction in a plasma.[2] The physical situation is as follows. A plasma has applied to it a constant, uniform magnetic field. The plasma is placed in a cylindrical microwave cavity that is excited so that an alternating electric field is established transverse to the magnetic field. It is found that the plasma constricts to a diameter that is such that the density of the plasma, or the plasma frequency, depends on the value of the magnetic field and the applied frequency of the electric field. For plane geometry, that is, for a plasma confined between two infinite parallel plates, Magda Erickson obtained $\omega_p^2 = \omega^2 - \omega_B^2$, where ω_p is the plasma frequency, and ω_B is

the cyclotron frequency. For cylindrical geometry, that is, for a plasma confined in a cylinder, the result was $\omega_p^2 = 2\omega(\omega-\omega_B)$.

The purpose of this report is to investigate this problem by using the transport equations and to show that Magda Erickson's results are easily obtained, although Ward's comment[2] that "the cause of the constriction is still unknown" remains valid.

We shall use the continuity equation, the linearized momentum equation, and Poisson's equation.

$$\partial n_1/\partial t + \nabla \cdot \vec{\Gamma} = 0 \tag{1}$$

$$\partial\vec{\Gamma}/\partial t + \frac{kT}{m}\nabla n_1 \pm e/m\, n_o \vec{E} + \vec{\omega}_B \times \vec{\Gamma} = 0 \tag{2}$$

$$\nabla \cdot \vec{E} = 4\pi e \left(n_1^+ - n_1^-\right) \tag{3}$$

Here, the plus sign refers to electrons, the minus, to ions; and $\vec{\omega}_{B\mp} = \mp eB_o/mc$, with B_o = constant, applied magnetic field. The particle density is written $n = n_o + n_1$, where n_o is the constant desnity, independent of space and time, and n_1 is the perturbed density $\left(\text{we have taken } n_o^+ = n_o^-\right)$. $\vec{\Gamma}$ is the particle flux vector, and, for simplicity, we have written the pressure as nkT, where T is a constant temperature. In this report, we shall assume that $\vec{\Gamma}$ is not a function of z, the direction of the constant magnetic field, and that $\nabla \times \vec{E} \approx 0$.

Taking the divergence and the curl of Eq. 2 and using Poisson's equation, we obtain the following relations:

$$\partial\nabla\cdot\vec{\Gamma}/\partial t + kT/m\nabla^2 n_1 \pm \frac{4\pi e^2 n_o}{m}\left(n_1^+ - n_1^-\right) - \vec{\omega}_{B_\mp}\cdot\nabla\times\vec{\Gamma} = 0 \tag{4}$$

$$\partial\nabla\times\vec{\Gamma}/\partial t + \vec{\omega}_{B_\mp}(\nabla\cdot\Gamma) = 0. \tag{5}$$

If we allow n_1, Γ, and E to vary with time as $e^{j\omega t}$ and define $\omega_p^2 = \frac{4\pi n_o e^2}{m}$, Eqs. 1, 4, and 5 combine to give the following relations for the spatial part of the perturbed electron and ion densities.

$$\frac{kT_-}{m_-}\nabla^2 n_1^- + \left(\omega^2 - \omega_{B_-}^2 - \omega_{p_-}^2\right)n_1^- + \omega_{p_-}^2 n_1^+ = 0 \tag{6}$$

$$\frac{kT_+}{m_+}\nabla^2 n_1^+ + \left(\omega^2 - \omega_{B_+}^2 - \omega_{p_+}^2\right)n_1^+ + \omega_{p_+}^2 n_1^- = 0 \tag{7}$$

We shall not consider these equations in detail but simplify matters even more to

see what essential information is contained in them.

We hold the ions stationary by letting $m_+ \to \infty$; then $n_1^+ \to 0$. We shall also consider the particular geometry of secondary importance, and neglect the $kT/m_- \nabla^2 n_1^-$ terms. The final Erickson results did not depend on temperature. We are left with the condition $\omega_{p_-}^2 = \omega^2 - \omega_{B_-}^2$, or if we define

$$\omega_{p_-}^2 \Big/ \omega^2 = a^2 \quad \text{and} \quad \omega_{B_-}^2 \Big/ \omega^2 = \beta^2, \tag{8}$$

we obtain

$$a^2 = 1 - \beta^2 \tag{9}$$

In Table X-1 experimental results for cylindrical geometry and data calculated from Erickson's formula for this geometry and from Eq. 9, which is her result for plane geometry, are listed. The observed values of β and a^2 were obtained from Erickson's report.[1] The values of ω_p^2 (calculated) as previously determined have not been used in obtaining a^2 according to the Erickson formula. For the sake of comparison, we also tabulate $\epsilon = 100 \times [a^2(\text{calculated}) - a^2(\text{observed})]/a^2(\text{observed})$.

From the data of Table X-1 we conclude that the formula for the plane case gives better, or at least as accurate, results as that for the cylindrical case.

Table X-1. Data for plasma constriction.

B_o (gauss)	β	a^2_{obs}	$a^2_{cal}=(1-\beta^2)$ (plane)	$a^2_{cal}=2(1-\beta)$ (cylinder)	ϵ (plane)	ϵ (cylinder)
900	0.8755	0.2294	0.2304	0.2490	0.44	8.54
920	0.8949	0.1927	0.1992	0.2102	3.37	9.08
940	0.9144	0.1438	0.1639	0.1712	13.98	19.05
960	0.9339	0.1254	0.1228	0.1322	-2.07	5.42
980	0.9533	0.1101	0.0912	0.0934	17.17	-15.17

Note that there is an innate difficulty in comparing the two calculated values of a^2. The ratio of the two values is $a^2(\text{plane})/a^2(\text{cylinder}) = (1+\beta)/2$. All of the experimental values of β were approximately 0.9 and, therefore, the accuracy of the comparison is poor.

As a final comment we shall consider the time rate of change of the total energy density in the plasma, that is, the sum of the electric field energy density E_F and the

particle energy density E_p. We shall neglect temperature effects. We find that

$$d/dt\ E_F = \mathrm{Re}\ (j\omega E^2/8\pi) \tag{11}$$

$$d/dt\ E_p = -\left(\omega_p^2/\omega^2-\omega_B^2\right)\ \mathrm{Re}\ (j\omega E^2/8\pi). \tag{12}$$

The sum of Eqs. 11 and 12 is

$$d/dt\ (E_F+E_p) = \left(1-\omega_p^2/\omega^2-\omega_B^2\right)\ \mathrm{Re}\ (j\omega E^2/8\pi). \tag{13}$$

Hence, if we define the equilibrium condition as that for which the total energy density is a constant, Eq. 8 is obtained. This is not unexpected, for if we neglect the B associated with $\vec{E}$ and dot $\vec{E}$ into Maxwell's curl $\vec{B}$ equation, we obtain $\partial/\partial t\ E^2/8\pi + E\cdot J = 0$, which is identical with Eq. 13.

H. R. Radoski

References

1. Magda Erickson, Electrostriction in plasmas, Quarterly Progress Report No. 57, Research Laboratory of Electronics, M. I. T., April 15, 1960, pp. 15-20.

2. C. S. Ward, Anomalous constriction of low-pressure microwave discharges in hydrogen, Quarterly Progress Report No. 55, Research Laboratory of Electronics, M. I. T., October 15, 1959, pp. 5-8.